Journal of Alloys and Compounds 581 (2013) 585–589

Contents lists available at SciVerse ScienceDirect

Journal of Alloys and Compounds

journal homepage: www.elsevier.com/locate/jalcom

Formation of long-period stacking ordered phase only within grains in Mg–Gd–Y–Zn–Zr casting by friction stir processing

Q. Yang [a], B.L. Xiao [a], D. Wang [a], M.Y. Zheng [b], K. Wu [b], Z.Y. Ma [a,*]

[a] Shenyang National Laboratory for Materials Science, Institute of Metal Research, Chinese Academy of Sciences, 72 Wenhua Road, Shenyang 110016, China
[b] School of Materials Science and Engineering, Harbin Institute of Technology, 92 West Dazhi Street, Harbin 150001, China

ARTICLE INFO

Article history:
Received 1 June 2013
Received in revised form 10 July 2013
Accepted 10 July 2013
Available online 19 July 2013

Keywords:
Friction stir processing
Magnesium alloys
Long-period stacking ordered structure
Mechanical properties

ABSTRACT

Friction stir processing (FSP) was applied to Mg–Gd–Y–Zn–Zr casting, resulting in significant dissolution of large grain boundary eutectic β-Mg_3RE and long-period stacking ordered (LPSO) phases. A fine-grained structure with a grain size of ~2.4 μm was developed in the FSP sample. Besides, fine LPSO lamellae with a width of ~5 to ~200 nm were distributed only within the grains in the FSP sample, which is different from that observed in both solution-treated and other plastically deformed counterparts. Formation of such special structure is attributed to the high temperature severe plastic deformation generated by FSP. The FSP Mg–Gd–Y–Zn–Zr exhibited high mechanical properties with a yield strength of ~345 MPa and an elongation of ~21.5%. This study provides an effective way for mechanical property optimization in LPSO-contained magnesium alloys.

1. Introduction

Ever since the development of a rapidly solidified powder metallurgy (RS P/M) processed $Mg_{97}Zn_1Y_2$ alloy with a high tensile yield strength of 610 MPa and an appreciable elongation of 5% [1], Mg–Zn–RE (rare earth) alloys containing long-period stacking ordered (LPSO) phase have gained numerous attention in development of high strength magnesium alloys [2–9]. The LPSO phase can form both in the casting and after annealing, and can be distributed both within the grains and at the grain boundaries [5,6,10]. Studies on the strengthening effect of the LPSO phase revealed that, it can kink by any angle to promote homogeneous deformation, inhibit twinning [11], increase the critical resolved shear stress of basal slip and activate non-basal slip in the matrix [7,12]. Therefore, the LPSO phase is beneficial to both strength and ductility of magnesium alloys.

Many efforts have been made for mechanical property optimization in the Mg–Zn–RE alloys, such as alloy design, refinement of grains, LPSO phase and other second phases, and texture control [9,13–16]. Because the distribution of LPSO phase can be varied, different distributions of LPSO phase can exhibit different contributions to the strength and ductility of Mg–Zn–RE alloys. By changing the cooling rate of the homogenized Mg–Gd–Y–Zn–Zr alloy, Xu et al. [17] obtained varied distributions of LPSO phase and showed that, the lamellar-shaped LPSO phase within the grains could enhance the yield strength. The study by Wang et al. [18] revealed that the bulk-shaped LPSO phase distributed along the grain boundaries promoted the formation of equiaxed grains and enhanced the ductility, whereas the lamellar LPSO phase precipitating within the grains induced strip-shaped grains and improved the strength of the as-extruded Mg–9Gd–*x*Er–1.6Zn–0.6Zr alloys.

The distribution of LPSO phase at the grain boundaries can be easily obtained in the Mg–Zn–RE alloys [10,19–21], and its contribution to strength can be well clarified. However, due to the inevitable solute segregation (especially Zn) in ingot cast alloys, the distribution of LPSO phase within the grains is inevitably accompanied by the grain boundary LPSO phase in the as-cast, solution-treated, and even plastically-deformed alloys [14,17–19,22,23]. Thus, contribution of the LPSO phase within the grains to the strength and ductility of Mg–Zn–RE alloys cannot be fully identified, and this hinders the study of mechanical property optimization in LPSO-contained magnesium alloys.

By the RS P/M method, the LPSO phase can be distributed only within the grains in Mg–Zn–RE alloys [24,25]. However, the unavoidable contamination of oxidation makes the RS P/M alloys incomparable with the ingot cast counterparts. Moreover, for both heat-treated and plastically-deformed Mg–Zn–RE alloys, a solution treatment at ~500 °C for ~6–35 h is an inevitable process. Such a solution treatment not only is time consuming, but also results in surface oxidation and grain growth. Therefore, a simple and effective technique that can achieve the distribution of LPSO phase only within the grains in ingot cast Mg–Zn–RE alloys is desired in the study of LPSO distribution effect on the mechanical properties.

* Corresponding author. Tel./fax: +86 24 83978908.
E-mail address: zyma@imr.ac.cn (Z.Y. Ma).

0925-8388/$ - see front matter © 2013 Elsevier B.V. All rights reserved.
http://dx.doi.org/10.1016/j.jallcom.2013.07.065

Friction stir processing (FSP), based on the concepts of friction stir welding (FSW), has been demonstrated to be an effective technique for microstructural modification [26,27]. The severe plastic deformation at high temperature generated by FSP can significantly refine the grains by dynamic recrystallization, dissolve the eutectics and refine large particles, alleviate severe composition segregation in cast magnesium alloys in just several seconds [28–30]. In this case, FSP has the combined function of solution treatment and plastic deformation [28,30].

In this study, FSP was applied to a cast Mg–Gd–Y–Zn–Zr alloy. The aim is to develop a fine-grained structure with the LPSO phase only within the grains and enhance the mechanical properties of the Mg–Gd–Y–Zn–Zr casting by FSP.

2. Experimental

Six millimeter thick Mg–9.4Gd–4.1Y–1.2Zn–0.4Zr (wt.%) cast plate was subjected to FSP. Two-pass FSP was carried out with a tool rotation rate of 2500 rpm and a traverse speed of 100 mm min^{-1} for the first pass, and a rotation rate of 800 rpm and a traverse speed of 100 mm min^{-1} for the second pass. A tool with a shoulder 20 mm in diameter and a threaded conical pin 8 mm in diameter and 4.0 mm in length was used.

Microstructural characterization was conducted in the cross section of the processed zone by X-ray diffraction (XRD), optical microscopy (OM), field-emission scanning electron microscopy (FE-SEM, LEO SUPRA 35) and transmission electron microscopy (TEM, Tecnai F20) equipped with energy-dispersive spectroscope (EDS). Thin foils for TEM were prepared by low energy ion milling. The texture was examined by electron backscatter diffraction (EBSD) analysis using an HKL Channel 5 System equipped in a scanning electron microscope. Coordinate axes of the pole figures are indicated using the processing direction (PD), transverse direction (TD) and normal direction (ND) of the plate.

Tensile specimens with a gauge length of 2.5 mm, a gage width of 1.4 mm and a gage thickness of 0.8 mm were machined in the cross section perpendicular to the FSP direction, with the gage being centered in the processed zone. Tensile tests were conducted at a strain rate of 1×10^{-3} s^{-1} using an Instron 5848 microtester. At least three specimens were used to obtain consistent stress–strain curve.

3. Results and discussion

3.1. Microstructure

Fig. 1 shows XRD patterns of the as-cast and FSP Mg–Gd–Y–Zn–Zr alloys. The as-cast alloy consisted mainly of α-Mg and eutectic β-Mg_3RE phase. Besides, weak peaks of the LPSO phase were detected. However, neither β nor LPSO phase was detected in the FSP alloy, indicating significant dissolution of the β and LPSO phases during FSP.

OM image of the as-cast alloy shows the dendritic α-Mg grains ~97 μm in size and the eutectic β phase in a black contrast (Fig. 2(a)). Besides, a small amount of the block-shaped LPSO phase with a gray contrast was observed at the grain boundaries. EDS analysis revealed that the average composition of β phase was Mg-10.5 ± 1.8Gd-7.2 ± 1.7Zn-6.8 ± 1.1Y (at.%), with obvious segregation of Zn. Selected area electron diffraction (SAED) patterns of the LPSO phase revealed that there were spots at positions of $n/6$ $(002)_{Mg}$ (n is an integer) (Fig. 2(b)), indicating the 18R structure [2]. Furthermore, as shown in Fig. 2(c), profuse stacking faults (SFs) were distributed within the grains. Zn was seldom detected within the grains.

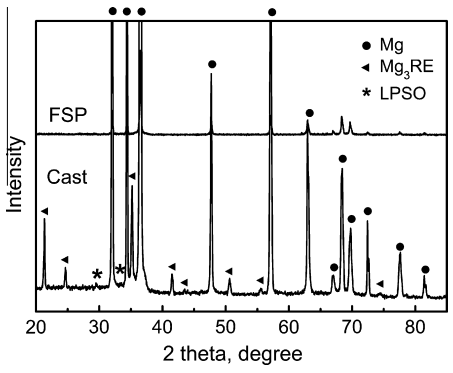

Fig. 1. XRD patterns of the Mg–Gd–Y–Zn–Zr alloy.

Microstructure of the FSP alloy consisted of uniform and fine dynamically recrystallized grains of ~2.4 μm with no grain boundary particles, furthermore, the fine lamellae within the grains could be observed (Fig. 3(a)). The back scattered electron (BSE)–SEM image in Fig. 3(b) revealed that, except for a few cuboid-shaped compounds commonly observed in Mg–Gd–Y based alloys, no decoration of other second phase particles was observed at the grain boundaries. This suggested that, no grain boundary particles existed in the FSP Mg–Gd–Y–Zn–Zr alloy.

The bright-field TEM image in Fig. 4(a) further confirmed the absence of grain boundary phase, and neither the β nor the metastable precipitates were detected within the grains. However, the fine lamellae with a width ranging from ~5 to ~200 nm were observed within the grains, and SAED patterns indicated that they were mainly the 18R LPSO phase. Further observation by high-resolution TEM (HRTEM) with the electron beam parallel to $<1\,1\,2\,0>_{\alpha}$ in Fig. 4(b) revealed that, the LPSO phase consisted of ABCA-type building blocks that were arranged in the same direction in each grain. Most building blocks were separated by two close-packed α-Mg layers to form the 18R structure as seen in the left side of Fig. 4(b), which is consistent with the distinct SAED patterns in Fig. 4(a). Besides, the separation of four α-Mg layers occasionally occurred both in adjacent two and three building blocks, as seen in the middle and right side of Fig. 4(b). Note that combination of the three building blocks in the middle of Fig. 4(b) could make the 24R structure, as reported previously [3,31,32]. Other types of LPSO phase were not observed.

Previous studies on FSP of magnesium castings indicated that FSP had the combined function of solution treatment and plastic deformation, as both dissolution of the eutectics and grain refinement were achieved during FSP [28,30]. It is interesting to note that although the grain size in the FSP Mg–Gd–Y–Zn–Zr alloy is equivalent to that in the plastically-deformed counterparts [13,19], the distribution of LPSO phase in these processed alloys is different. In the solution-treated and subsequent plastically-deformed Mg–Gd–Zn based alloys, the LPSO phase was inevitably distributed at the grain boundaries [13,18,22,33]. However, in the present FSP Mg–Gd–Y–Zn–Zr alloy, the LPSO phase was distributed only within the grains.

Formation of the special microstructure in the FSP Mg–Gd–Y–Zn–Zr alloy could result from the unique deformation process of FSP. It is acknowledged that formation of the LPSO phase is a process of high temperature diffusion and periodic segregation of Zn and RE atoms in the adjacent $(0\,0\,0\,1)_{Mg}$ layers, higher temperature could enhance this process [6,10,25]. Moreover, the LPSO phase can both be transformed from the β phase at the grain boundaries and precipitate from the matrix upon annealing in the Mg–Gd–Zn based alloys [6,10].

During solution treatment of the Mg–Gd–Zn based castings, the solute segregation in the grain boundary eutectics results in preferred formation of the LPSO phase at the grain boundaries due to much shortened diffusion distance. As a result, precipitation of the LPSO phase within the grains is hindered due to the lack of solute atoms (especially Zn). Further formation of the LPSO phase within the grains required much longer time and higher temperature due to low diffusion rate of the solutes. During subsequent plastic deformation, the already formed grain boundary LPSO phase could only be refined and precipitation of the LPSO phase is still restricted due to the lack of Zn within the grains. In this case, the inevitable distribution of LPSO phase at the grain boundaries is

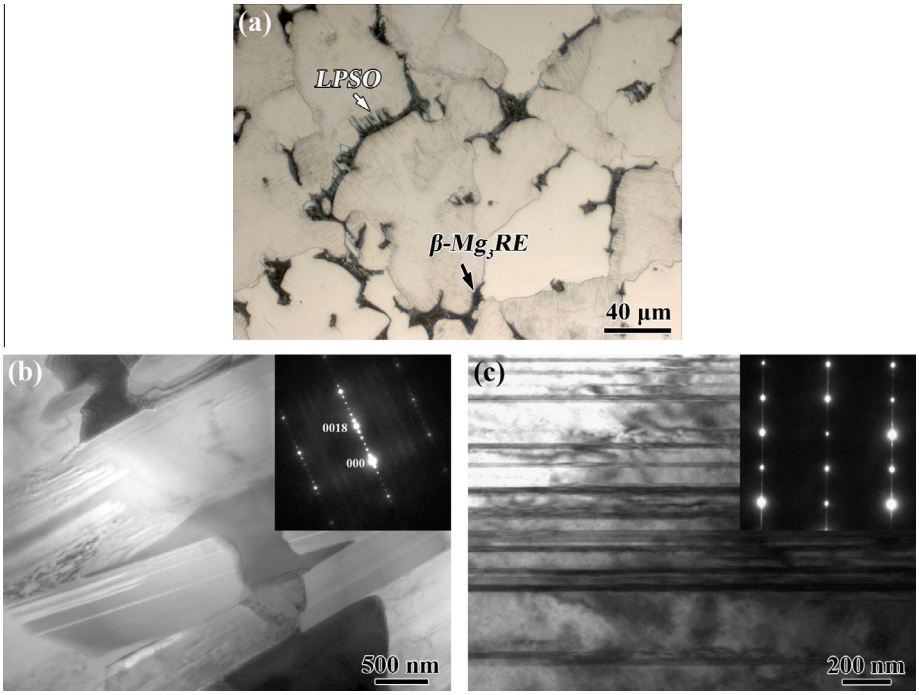

Fig. 2. Microstructure of the as-cast Mg–Gd–Y–Zn–Zr alloy: (a) OM image, TEM images of (b) the grain boundary LPSO phase and (c) the stacking faults within the grains.

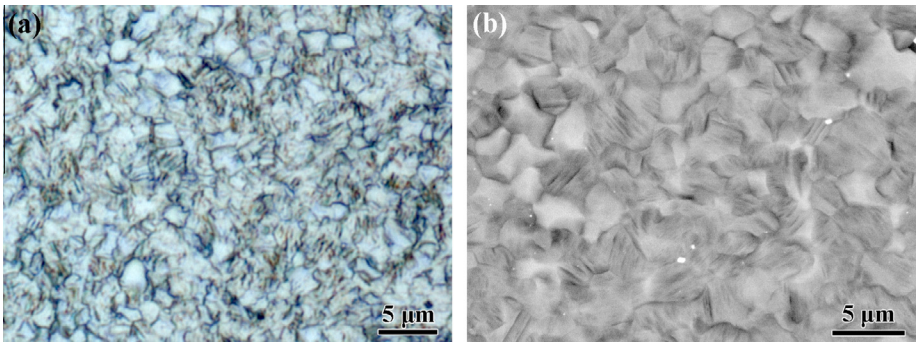

Fig. 3. (a) OM and (b) BSE–SEM images of the FSP Mg–Gd–Y–Zn–Zr alloy.

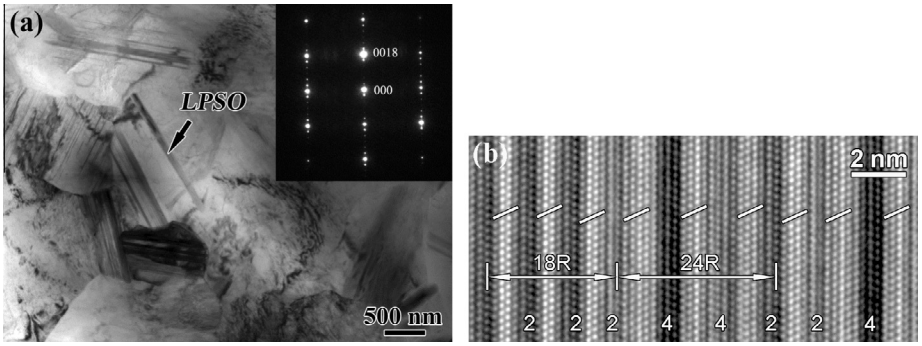

Fig. 4. (a) Bright-field TEM image of the FSP Mg–Gd–Y–Zn–Zr alloy; (b) HRTEM image of the LPSO phase with the electron beam parallel to $<11\bar{2}0>_{\alpha}$.

observed in the Mg–Gd–Zn based alloys processed by conventional methods.

Our previous study on the FSP Mg–Gd–Y–Zr alloy revealed that, the severe plastic deformation and high temperature generated during FSP could result in dissolution of the eutectic β-Mg_5(Gd,Y) particles [28]. Therefore, for the present Mg–Gd–Y–Zn–Zr casting with similar particle dissolution temperature and FSP condition, FSP can also result in intense material mixing, breakup and dissolution of the eutectic β-Mg_3RE and LPSO particles in the casting. Therefore, the severe solute segregation was eliminated, and the

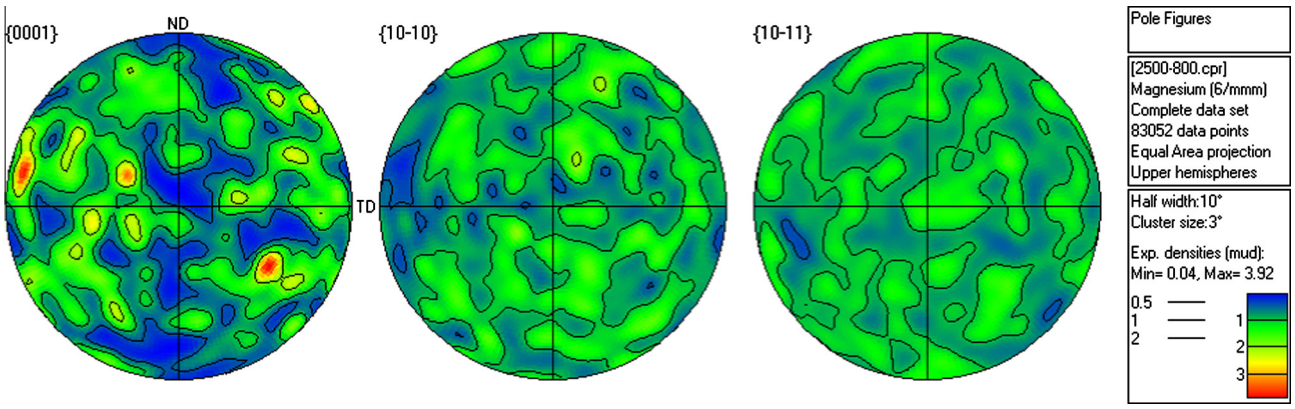

Fig. 5. Pole figures of the FSP Mg–Gd–Y–Zn–Zr alloy.

Table 1
Tensile properties of Mg–Gd–Y–Zn–Zr alloy.

Condition	YS (MPa)	UTS (MPa)	El (%)
As-cast	187 ± 5.2	249 ± 5.5	7.9 ± 0.6
FSP	345 ± 5.5	380 ± 9.9	21.5 ± 3.3

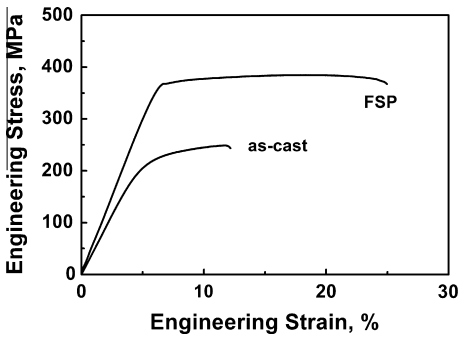

Fig. 6. Engineering stress–strain curves of the as-cast and FSP Mg–Gd–Y–Zn–Zr alloy.

solutes (especially Zn) were distributed uniformly in the matrix. Consequently, the LPSO phase precipitated during high temperature annealing, and was distributed only within the grains.

It is worth noting that, different from the commonly observed 14H structure in the solution-treated and plastically-deformed Mg–Gd–Zn based alloys [4,6,10,34], the 18R and even 24R structures formed in the FSP Mg–Gd–Y–Zn–Zr alloy. Similar polytypes of LPSO phase were observed in the RS P/M Mg–Zn–Y alloys [3,31]. Recently, Zhu et al. [32] observed the formation of 24R in 18R structure in a cast Mg–Zn–Y alloy after annealing at 500 °C for 1 h, and proposed that formation of 24R provided a simple path for the transformation from 18R to 14H. Accordingly, the LPSO phase in the present FSP alloy is in a non-equilibrium state and would transform to the 14H upon further annealing.

Fig. 5 reveals that different from the concentrated basal texture with the *c* axis aligning approximately along the processing direction developed in FSP conventional magnesium alloys [35–37], a weak and much scattered basal texture was developed in the FSP Mg–Gd–Y–Zn–Zr alloy. Similar weak basal texture was reported in plastically-deformed Mg–Gd–Zn alloy [13], and should be attributed to the contribution of RE elements that weaken the texture of magnesium alloys [38,39].

3.2. Mechanical properties

Table 1 summarizes the mechanical properties of the as-cast and FSP Mg–Gd–Y–Zn–Zr alloys, and the typical tensile curves are shown in Fig. 6. Due to the coarse grains and large grain boundary particle networks, the as-cast alloy exhibited low strengths and elongation. In contrast, the FSP alloy revealed substantially improved strengths and elongation, with a yield strength (YS) of ~345 MPa, an ultimate strength (UTS) of ~380 MPa and a large elongation to failure of ~21.5%. However, compared with the as-cast alloy, the FSP alloy exhibited a weak work hardening behavior during the whole deformation process.

As shown in Fig. 7(a), the brittle fracture characterized by deep cleavage steps and small cleavage facets occurred for the as-cast sample. In contrast, equiaxed and fine dimples were obviously

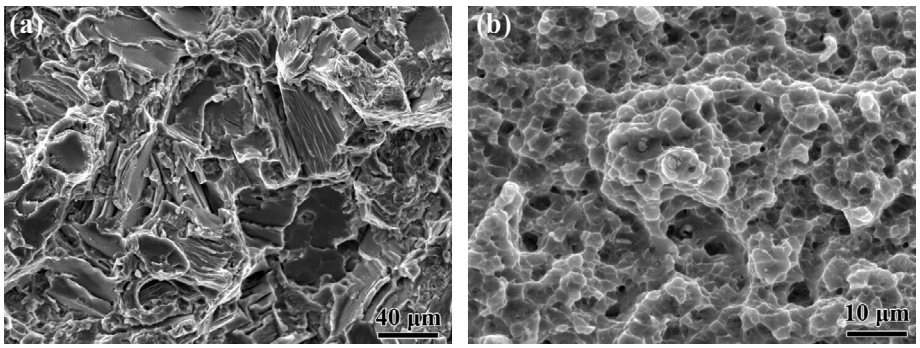

Fig. 7. Fractographs of (a) as-cast and (b) FSP Mg–Gd–Y–Zn–Zr alloy.

observed on the fracture surface of the FSP sample (Fig. 7(b)), indicating a good ductility.

In general, the mechanical properties of magnesium alloys are strongly influenced by the grain size based on the Hall-Petch relationship, the texture through its effect on activation of slip systems, and the second phase by dispersion and precipitation strengthening. The fine grains of ~2.4 μm can enhance both strength and ductility significantly in the FSP sample compared with the as-cast sample. Besides, Stanford and Barnett stated that the weak texture developed in magnesium alloys can lead to easy basal slip, resulting in enhanced ductility but reduced YS [40,41]. Therefore, the weak basal texture developed in the FSP sample can enhance the ductility. Furthermore, it was confirmed by both experimental observation and first-principle study that, the LPSO phase is effective in hindering basal slip and activating non-basal slip [7,12]. The suppression of basal slip enhances the YS, and the activation of non-basal slip promotes homogeneous deformation, leading to enhanced ductility. Therefore, the LPSO phase within the grains in the FSP sample also plays an important role in enhancing the mechanical properties. Namely, fine grains, weak texture, and LPSO phase within the grains contributed to the high mechanical properties in the FSP Mg–Gd–Y–Zn–Zr alloy.

The weak work hardening behavior of the present FSP Mg–Gd–Y–Zn–Zr alloy might be caused by the fine grains and the distribution of LPSO phase only within the grains, both of these can activate the non-basal slip that is crucial for dislocation recovery during tension. Detailed study is required to understand the effect of LPSO distribution on the mechanical properties and deformation behavior of the Mg–Zn–RE based alloys.

4. Conclusions

1. The Mg–Gd–Y–Zn–Zr casting was successfully friction stir processed. FSP resulted in significant grain refinement and dissolution of the large grain boundary β-Mg_3RE and LPSO particles in the casting.
2. The FSP Mg–Gd–Y–Zn–Zr alloy exhibited fine grains of ~2.4 μm, besides, fine LPSO lamellae with a width of ~5 to ~200 nm were distributed only within the grains.
3. The FSP Mg–Gd–Y–Zn–Zr alloy with a YS of ~345 MPa and an elongation of ~21.5%, exhibited significantly enhanced mechanical properties compared to the as-cast counterpart. FSP provides an effective way for mechanical property optimization in LPSO-contained magnesium alloys.

Acknowledgements

This work is supported by the National Natural Science Foundation of China under Grant Nos. 50901075 and 50890171, the National Basic Research Program of China under Grant No. 2011CB606301.

References

[1] A. Inoue, Y. Kawamura, M. Matsushita, K. Hayashi, J. Koike, J. Mater. Res. 16 (2001) 1894–1900.
[2] T. Itoi, T. Seimiya, Y. Kawamura, M. Hirohashi, Scripta Mater. 51 (2004) 107–111.
[3] M. Matsuda, S. Ii, Y. Kawamura, Y. Ikuhara, M. Nishida, Mater. Sci. Eng. A 393 (2005) 269–374.
[4] T. Honma, T. Ohkubo, S. Kamado, Acta Mater. 55 (2007) 4137–4150.
[5] Y. Kawamura, M. Yamasaki, Mater. Trans. 48 (2007) 2986–2992.
[6] M. Yamasaki, M. Sasaki, M. Nishijima, K. Hiraga, Y. Kawamura, Acta Mater. 55 (2007) 6798–6805.
[7] A. Datta, U.V. Waghmare, U. Ramamurty, Acta Mater. 56 (2008) 2531–2539.
[8] Y.M. Zhu, A.J. Morton, J.F. Nie, Acta Mater. 58 (2010) 2936–2947.
[9] M. Yamasaki, K. Hashimoto, K. Hagihara, Y. Kawamura, Acta Mater. 59 (2011) 3646–3658.
[10] W.J. Ding, Y.J. Wu, L.M. Peng, X.Q. Zeng, G.Y. Yuan, J. Mater. Res. 24 (2009) 1842–1854.
[11] M. Matsuda, S. Ii, Y. Kawamura, Y. Ikuhara, M. Nishida, Mater. Sci. Eng. A 386 (2004) 447–452.
[12] M. Matsuda, S. Ando, M. Nishida, Mater. Trans. 46 (2005) 361–364.
[13] C. Xu, S.W. Xu, M.Y. Zheng, K. Wu, E.D. Wang, S. Kamado, G.J. Wang, X.Y. Lv, J. Alloys Comp. 524 (2012) 46–52.
[14] M. Yamasaki, T. Anan, S. Yoshimoto, Y. Kawamura, Scripta Mater. 53 (2005) 799–803.
[15] K. Yamada, Y. Okubo, M. Shiono, H. Watanabe, S. Kamado, Y. Kojima, Mater. Trans. 47 (2006) 1066–1070.
[16] S. Yoshimoto, M. Yamasaki, Y. Kawamura, Mater. Trans. 47 (2006) 959–965.
[17] C. Xu, M.Y. Zheng, K. Wu, E.D. Wang, G.H. Fan, S.W. Xu, S. Kamado, X.D. Liu, G.J. Wang, X.Y. Lv, Mater. Sci. Eng. A 559 (2012) 364–370.
[18] J. Wang, P. Song, S. Huang, F. Pan, Mater. Sci. Eng. A 563 (2013) 36–45.
[19] L. Zheng, C. Liu, Y. Wan, P. Yang, X. Shu, J. Alloys Comp. 509 (2011) 8832–8839.
[20] T. Itoi, T. Inazawa, M. Yamasaki, Y. Kawamura, M. Hirohashi, Mater. Sci. Eng. A 560 (2013) 216–223.
[21] J. Wang, P. Song, X. Zhou, X. Huang, F. Pan, Mater. Sci. Eng. A 556 (2012) 68–75.
[22] K. Liu, J. Zhang, H. Lu, D. Tang, L.L. Rokhlin, F.M. Elkin, J. Meng, Mater Des. 31 (2010) 210–219.
[23] Y. Gao, Q. Wang, J. Gu, Y. Zhao, Y. Tong, D. Yin, J. Alloys Comp. 477 (2009) 374–378.
[24] Y. Kawamura, K. Hayashi, Mater. Trans. 41 (2001) 1172–1176.
[25] E. Abe, Y. Kawamura, K. Hayashi, A. Inoue, Acta Mater. 50 (2002) 3845–3857.
[26] R.S. Mishra, Z.Y. Ma, Mater. Sci. Eng. R 50 (2005) 1–78.
[27] Z.Y. Ma, Metal. Mater. Trans. A 39 (2008) 642–658.
[28] B.L. Xiao, Q. Yang, J. Yang, W.G. Wang, G.M. Xie, Z.Y. Ma, J. Alloys Comp. 509 (2011) 2879–2884.
[29] D. Zhang, M. Suzuki, K. Maruyama, Scripta Mater. 52 (2005) 899–903.
[30] A.H. Feng, Z.Y. Ma, Scripta Mater. 56 (2007) 397–400.
[31] E. Abe, A. Ono, T. Itoi, M. Yamasaki, Y. Kawamura, Philos. Mag. Lett. 91 (2011) 690–696.
[32] Y.M. Zhu, A.J. Morton, J.F. Nie, Acta Mater. 60 (2012) 6562–6572.
[33] Y.J. Wu, L.M. Peng, X.Q. Zeng, J. Mater. Res. 24 (2009) 3596–3602.
[34] K. Liu, J. Zhang, G. Su, J. Alloys Comp. 481 (2009) 811–818.
[35] Q. Yang, A.H. Feng, B.L. Xiao, Z.Y. Ma, Mater. Sci. Eng. A 556 (2012) 671–677.
[36] J. Yang, D. Wang, B.L. Xiao, D.R. Ni, Z.Y. Ma, Metal. Mater. Trans. A 44A (2012) 517–530.
[37] S.H.C. Park, Y.S. Sato, H. Kokawa, Metal. Mater. Trans. A 34A (2003) 987–994.
[38] J. Bohlen, M.R. Nürnberg, J.W. Senn, D. Letzig, S.R. Agnew, Acta Mater. 55 (2007) 2101–2112.
[39] K. Hantzsche, J. Bohlen, J. Wendt, K.U. Kainer, S.B. Yi, D. Letzig, Scripta Mater. 63 (2010) 725–730.
[40] N. Stanford, D. Atwell, A. Beer, C. Davies, M.R. Barnett, T.S.A. Uoya, K. Higashi, A. Inoue, T. Masumoto, Scripta Mater. 59 (2008) 772–775.
[41] N. Stanford, M. Barnett, Scripta Mater. 58 (2008) 179–182.